Enhancing the Bond Strength Between Glass Fibre Reinforced Polyamide 6 and Aluminium through µPlasma Surface Modification.

Jenkins, Michael; Che, Chang; Dashtbozorg, Ben; Dong, Hanshan

DOI:
10.2139/ssrn.4591488
10.1016/j.apsusc.2024.159734

Document Version
Publisher's PDF, also known as Version of record

Citation for published version (Harvard):
Jenkins, M, Che, C, Dashtbozorg, B & Dong, H 2024, 'Enhancing the Bond Strength Between Glass Fibre Reinforced Polyamide 6 and Aluminium through µPlasma Surface Modification.', *Applied Surface Science*, vol. 657, 159734. https://doi.org/10.2139/ssrn.4591488, https://doi.org/10.1016/j.apsusc.2024.159734

Applied Surface Science 657 (2024) 159734

Contents lists available at ScienceDirect

Applied Surface Science

journal homepage: www.elsevier.com/locate/apsusc

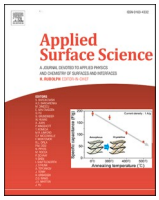

Full Length Article

Enhancing the bond strength between glass fibre reinforced polyamide 6 and aluminium through μPlasma surface modification

Chang Che *, Xueqi Zhu, Behnam Dashtbozorg, Xiaoying Li, Hanshan Dong, Mike J. Jenkins

School of Metallurgy & Materials, University of Birmingham, Birmingham B15 2SE, UK

ARTICLE INFO

Keywords:
μPlasma
Thermoplastic
Wettability
Bond strength
Aluminium
Ageing

ABSTRACT

Thermoplastic polymers generally exhibit relatively low surface energies and this often results in limited adhesion when bonded to other materials. Plasma surface modification offers the potential to functionalise the polymer surfaces, and thereby enhance the bond strength between dissimilar materials. In this study, glass fibre reinforced polyamide 6 (GFPA6) was modified using a novel μPlasma surface treatment technique and the effectiveness of the adhesive bond with aluminium was evaluated. The treated GFPA6 surfaces were characterised using atomic force microscopy (AFM), Raman spectroscopy, contact angle measurements, surface free energy calculations and wetting envelope analysis. The results show that there was a near exponential growth in root mean square roughness with increasing treatment scans. A significant increase in carbonyl and amide functionality on the polymer surface was observed using Raman spectroscopy. The total surface energy was found to increase from 42.2 mN/m to 67.6 mN/m following a single treatment scan. Significant increases in the tensile shear strength were observed up to 10 treatment scans, going from 1 kN to 2.3 kN, but no further increase was observed with additional treatment scans. These observations, coupled with the atmospheric nature of the technique, points to great potential as a rapid, on-line, and effective, polymer surface treatment technique.

1. Introduction

Reduction in CO_2 emissions from motor vehicles is being achieved through a variety of means, one of which is vehicle lightweighting to improve fuel efficiency. A common approach taken to reach this goal is to replace structural metallic components, such as the floor, bonnet, roof and door panel of the vehicle, with parts [1] made from light glass fibre reinforced polymer matrix composites [2]. The polymer matrix can be a thermoset (e.g. an epoxy system) or thermoplastic (e.g. polyamide) [3]. While both these matrices offer a route to a reduction in weight, thermoplastic matrices offer significant advantages over thermosets in that they can be recycled and the part production time is significantly reduced [4,5]. In the context of the automotive (and aerospace) industry, an important thermoplastic composite is glass fibre reinforced polyamide 6 (GFRPA6), which exhibits good thermal stability and high tensile strength [6,7].

Often there is a need for thermoplastic composites to be joined with metals [8]. These hybrid structures facilitate the design of parts that not only exhibit increased strength, stiffness, and resistance to crack-induced physical damage, but also yield weight reduction [9]. Numerous approaches have been developed for the joining of polymers and metals, with mechanical fastening being the most traditional method [10]. However, problems can arise because of the use of mechanical fastening methods, for example, the drilling process concentrates stresses at the location of rivets or screws, which are then prone to cracking when high loads are applied [11]. In addition, the presence of bolts can increase the weight of the structure and compromise weather-sealing.

Adhesive bonding provides an alternative approach to the joining of materials and offers the potential for achieving better seals and defect-free connection between dissimilar materials. In addition, it eliminates the needs for mechanical components such as rivets and screws, thereby reducing both the stress concentrations in the joints and the weight in the hybrid structures [9]. To achieve a good structural bond, epoxy-based adhesives are often employed, but prior treatment such as surface modification of the thermoplastic surface are normally required to improve their surface adhesive properties before the adhesive bonding of the materials. This is necessary because thermoplastic surfaces

* Corresponding author.
E-mail addresses: chechang1010@gmail.com (C. Che), xxz172@bham.ac.uk (X. Zhu), b.dashtbozorg@bham.ac.uk (B. Dashtbozorg), x.li.1@bham.ac.uk (X. Li), h.dong.20@bham.ac.uk (H. Dong), m.j.jenkins@bham.ac.uk (M.J. Jenkins).

https://doi.org/10.1016/j.apsusc.2024.159734
Received 11 September 2023; Received in revised form 29 January 2024; Accepted 19 February 2024
Available online 22 February 2024

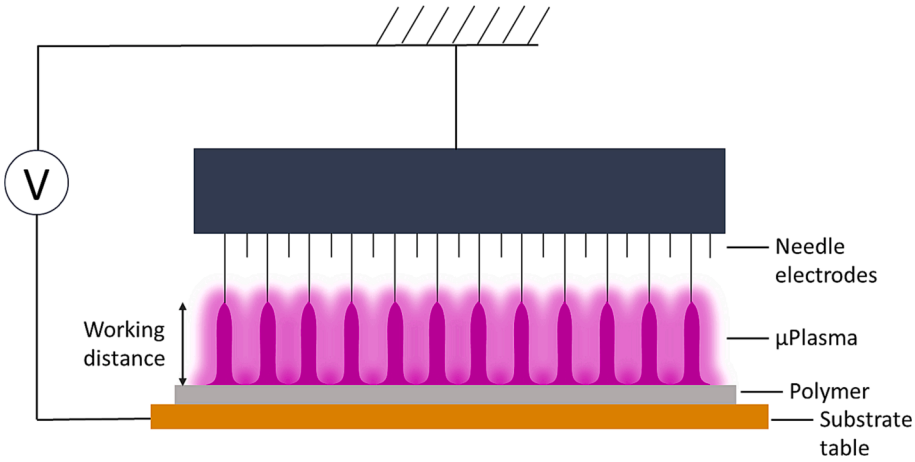

Fig. 1. An illustration of the µPlasma printing head with 24 needle electrodes.

typically have low surface free energies, which makes them difficult to wet, and therefore, they demonstrate poor adhesive properties [12]. A range of studies have confirmed that plasma treatments can improve the wettability, and therefore, adhesive properties of polymer surfaces [13–16]. In addition, it has been reported that plasma treated surfaces can improve the bonding strength between polymers and metals [17,18]. Unlike conventional plasma treatment systems, which require vacuum systems to operate, new µPlasma treatments can be performed under atmospheric pressure. As a result, the need for vacuum systems is eliminated, leading to increased treatment scalability, reduced treatment durations, and lower costs. µPlasma surface modification also allows for the local treatment of polymers and the design of surface patterns [19], which increases energy efficiency, as only the desired regions are treated. However, it has been reported previously that as is the case for other plasma treatments, the effects of µPlasma treatment are non-permanent. A post-treatment ageing process occurs that results in a significant decrease of surface wettability of the treated surface within the first 80 min after µPlasma treatment [20].

To the best of the authors knowledge, to date no previous studies have reported on the effect of plasma surface treatment on the adhesive bonding between glass fibre reinforced polyamide 6 (GFPA6) and aluminium. Therefore, the aim of this study is to characterise the effect of µPlasma surface modification of GFPA6 on the bond strength of epoxy-adhered GFPA6-aluminium joints. A tensile lap-shear test was selected for the mechanical characterisation and the influence of treatment repetitions (1, 10 and 20 µPlasma treatment scans) on the bond strength was assessed. A range of microscopy-based techniques were deployed in order to characterise the polymer surfaces and the changes in surface wettability of GFPA6 were determined via contact angle measurements, surface free energy calculations and wetting envelope analysis. Moreover, the study seeks to explore the significance of the post-treatment ageing process that has been reported previously [20] and understand its implications for the joining procedure.

2. Materials and methods

2.1. Materials

The glass fibre reinforced polyamide-6 (GFRPA6) used in this study was a Celstran@CFR-TP PA6 GF60-03 tape (GFPA6, Celanese Corporation, Dallas, TX, USA). The GFPA6 is composed of 60 wt% uniaxial long glass fibre reinforced and 40 wt% polyamide 6 and has a tensile strength of 240 MPa. A AA6082-T6 aluminium alloy (London, Smiths Metal Centres Ltd, UK), with a yield tensile strength of 270 MPa, was used as the other dissimilar material for joining. The alloying composition of the AA6082-T6 was 0.7–1.3 wt% Si, 0.6–1.2 wt% Mg, 0.4–1.0 wt% Mn, 0–0.5 wt% Fe, 0–0.25 wt% Cr, 0–0.2 wt% Zn, 0–0.1 wt% Ti, 0–0.1 wt% Cu. The two materials were joined together using MG Chemical 9200 FR Liquid Epoxy Adhesive (Corby, RS Components Ltd, UK). This adhesive system is reported to exhibit a tensile shear strength of 10 N/mm^2 (with aluminium). The protocol associated with the joining method is described in detail in §2.5.

2.2. µPlasma treatment

The GFPA6 surfaces were cleaned using ethanol and dried in air. After cleaning. µPlasma modification was performed using a Roth & Rau Pixdro LP50 plasma inkjet printer (InnoPhysics, Eindhoven, The Netherlands). The print-head (InnoPhysics POD24) within the device was connected to an alternative current power supply with 24 needles, as shown in Fig. 1. Previously published treatment settings for the surface modification of GFPA6 surface were used within this study [20]. For convenience, the optimal parameters were found to be as follows; an accelerating voltage of 7 kV, a printing rate of 20 mm/s, and a working distance from the sample surface to the tips of the printing needles of 100 µm.

2.3. Atomic force microscopy (AFM)

Atomic force microscope (AFM; Dimension 3100, Bruker, Billerica, USA) was used for surface morphology examination of the materials. The AFM was operated with a silicon nitride cantilevers (PPP-NCHR, tip radius $<$ 10 nm, length 125 um, resonant frequency 330 kHz, Nanosensor, Apex Probes Ltd, UK) under a tapping mode. The cantilevers were cleaned using an ethanol rinse and exposure to UV-zone for 10 mins before each scan. The scans were acquired on three different locations on each sample surface with a scan area of 17 µm x 17 µm. 3D height profiles and root mean square (RMS) roughness measurements were obtained using the (Gwyddion, SourceForge, San Diego).

2.4. Contact angle measurements

The contact angles of GFPA6 surfaces were measured using the sessile drop method. An experimental apparatus conforming to the ISO 19403–2:2020 standard [21] was utilised, where a camera connected to a monitor, a height (z-axis) adjustable sample stage, and an adjustable light source were aligned in a straight line to ensure measured contact angles were always obtained at the same angle. The measurements were performed under the ambient conditions using deionised water as the test liquid. Water droplets with a volume of 6 µL were carefully deposited onto the sample surfaces using a calibrated pipette. Ten repeat measurements were carried out on each sample, with both left and right

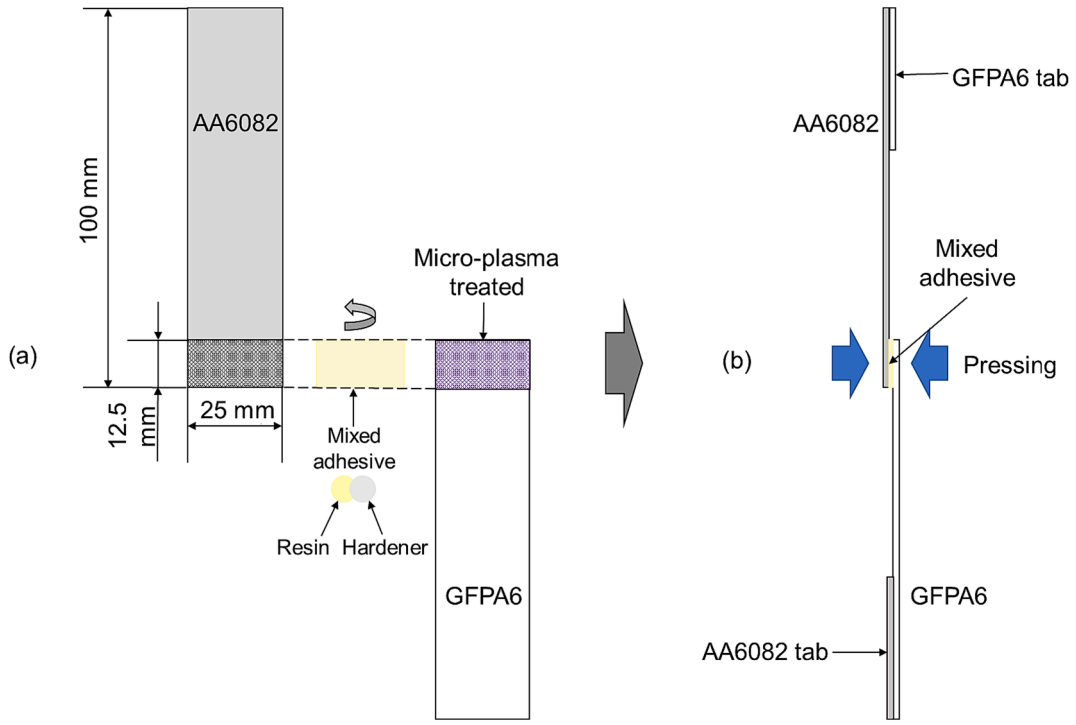

Fig. 2. A schematic illustration of (a) the joining method and sample size, and (b)the specimen for tensile lap-shear test after joining.

contact angles being used to ensure an accurate average contact angle measurement. The contact angle images were analysed using the Ossila contact angle measurement software (Ossila Ltd, Sheffield, UK).

2.5. Joining method

The GFPA6 and AA6082 samples were cut into 100 × 25 mm pieces. Prior to joining, the AA6082 plates were roughened using #120 grit SiC paper. To ensure uniform roughness on all samples, surfaces were ground horizontally and vertically, 15 times each. The ground AA6082 materials were then ultrasonically cleaned in acetone for 5 min to remove loose debris. The GFPA6 material surfaces were treated using μPlasma before the joining. In this study, the two materials (GFPA6 and AA6082) were joined together using an epoxy adhesive that was made of two components (resin and hardener). The two parts were well mixed in a 1:1 ratio, with a mass of 0.1 ± 0.001 g for each part.

The joining procedure is illustrated in Fig. 2. The mixed adhesive was evenly applied on the GFPA6 material surface immediately after μPlasma treatment, before joining with the AA6082, with joining area (plasma treated) of 12.5 mm × 25 mm. The joined materials were then cured in air at room temperature for 24 h before tensile testing was carried out. Expediting the joining process was deemed to be of significant importance because it has been previously reported that the effects of plasma surface treatment are not permanent in that a post-treatment ageing process takes place in the hours that follow the treatment [20].

2.6. Tensile lap-shear test

Uni-axial tensile lap-shear tests were conducted using an Instron 3367 tensile testing system (Instron, Massachusetts, US) with a load cell of 30 kN. The testing specimen are shown in Fig. 2 (a), which follows the EN ISO 4587 tensile lap-shear test standard. A tab was applied on each side to ensure parallel tensile testing was performed. The tests were carried out using a crosshead speed of 0.2 mm/min and tests were repeated 6 times for each variable (untreated and μPlasma treated one, 10 and 20 treatment scans).

2.7. Image segmentation

The coverage of the adhesive on broken GFPA6 surfaces after failure was analysed using the TWS (trainable Weka segmentation) plugin for Image J (Version 1.54c, Bethesda, Maryland, USA). Prior to the image segmentation, the adhesive area and polymer surface area were distinguished as two different classes by training classifier. This was done by drawing freehand lines on the adhesive area and set as class 1, while the polymer surface area was as class 2. The percentage of total area was then calculated using Image J.

2.8. Scanning electron microscopy (SEM)

A TM3030 SEM (Hitachi High-Technologies Corporation, Tokyo, Japan) was used to observe surface morphology of samples after tensile testing. Prior to SEM imaging, the sample surfaces were gold sputter coated using an EMITECH K550 Sputter Coater (EMITECH, Kent, UK) at 25 mA for three minutes.

2.9. Raman spectroscopy

Raman spectra were obtained using a Raman Microscope (InVia Raman Microscope, Renishaw plc., Wotton-under-edge, UK) with a laser wavelength of λ = 488 nm and an excitation power of ~2 mW. A confocal microscope with × 50 objective was used to focus the laser beam onto the samples with a spot-diameter of about 865 nm. A Raman data set consisting of 289 spectrums were collected using Raman mapping (each spot with a size of 150 × 150 μm) in a grid pattern over an area of 2550 × 2550 μm on the sample surface. The spectra were then deconvoluted and analysed using Casa XPS, where the average of the 289 spectra was summarised.

3. Results

3.1. Effect of μPlasma modification on the surface morphology of GFPA6

The 3D surface morphology of untreated and μPlasma treated GFPA6

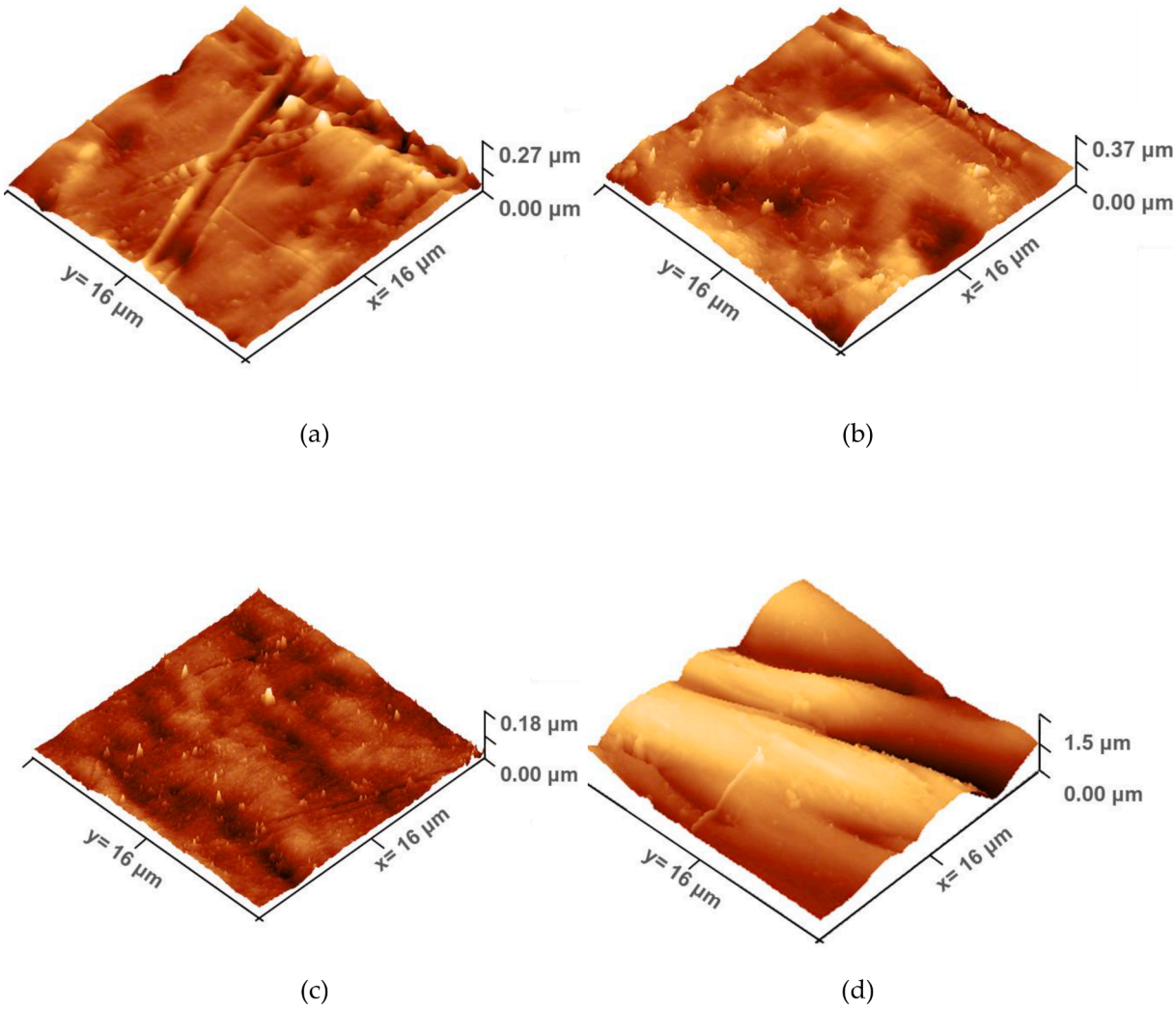

Fig. 3. 3D AFM images of surface morphology of (a) untreated, and µPlasma treated different times: (b) 1, (c) 10 and (d) 20.

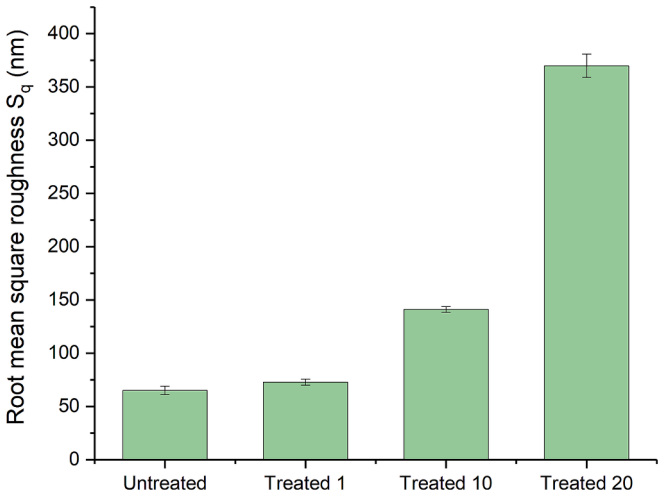

Fig. 4. Root mean square (RMS) roughness of untreated GFPA6, µPlasma treated once, 10 and 20 times.

was examined using AFM. As shown in Fig. 3, the surface morphology of the untreated GFRP6 appeared relatively smooth, and with a single µPlasma treatment, the resulting surface was not discernibly different. However, the surface roughness of GFPA6 increased significantly after 10 and 20 µPlasma treatment scans. It is notable that the material surface after 20 µPlasma treatment scans exhibited an uneven surface with distinctly raised fibres and pronounced grooves.

To quantify the observations in relation to surface roughness, the root mean square (RMS) roughness (S_q) was calculated, and the variations are illustrated in Fig. 4. Although no obvious roughness change can be observed in Fig. 3b, the value of S_q was revealed to increase with the increasing number of µPlasma treatment scans. The value of S_q initially increased from 65.0 nm to 72.8 nm following one µPlasma treatment scan, indicating a modest increase in surface roughness. More substantial increases were observed for 10 µPlasma treatment scans, with the value of S_q increased to 140.9 nm. The most significant increase in RMS roughness of the GFPA6 surfaces was observed for 20 µPlasma treatment scans with the value of S_q increased to 369.7 nm, which corresponds to an approximately 5 times greater roughness as the untreated surface. In summary, this demonstrated that the surface roughness of GFPA6 can be significantly increased following µPlasma modification, with the magnitude of the effect correlating with the number of µPlasma treatments. Significant increase of S_q was observed following 20 µPlasma treatment scans.

3.2. *Surface wettability*

Substantial enhancement in surface wettability was found following

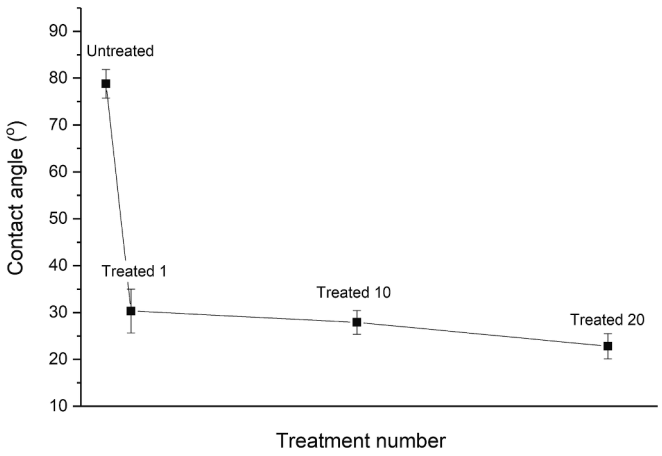

Fig. 5. Variation of the contact angle of the GFPA6 surface with the number of µPlasma treatment scans.

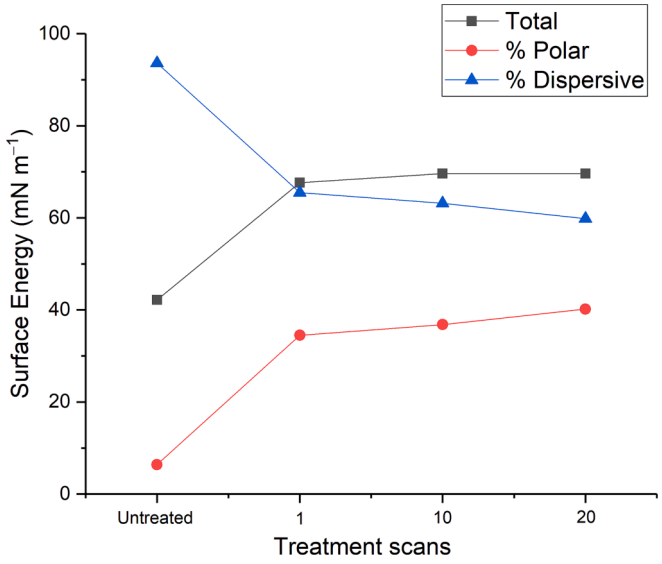

Fig. 6. Surface energy (total, polar and dispersive) of untreated GFPA6 and µPlasma treated GFPA6 with different treatment scans.

one µPlasma treatment, as evidenced by a 61.5 % reduction in contact angle (decreasing from 78.8° to 30.3°), as shown in Fig. 5. Following 10 and 20 µPlasma treatment scans, the contact angles decreased by 64.6 % (to 27.9°) and 71.1 % (to 22.8°), respectively, in comparison with the untreated surface. The results demonstrated that, beyond a single treatment scan, further µPlasma treatment scans did not significantly improve the surface wettability (despite an increase in roughness). To gain a better understanding of the surface wettability, the surface free energy was calculated using the contact angle results from tests with deionised water and diiodomethane. As shown in Fig. 6, the total surface free energy increased from 42.2 mN/m to 67.6 mN/m following a single µPlasma treatment, with increased contribution from polar surface energy components and decrease from dispersive components. The total surface free energy increased to 69.6 mN/m for 10 treatment scans, which suggests that the surface free energy change was limited beyond a single treatment scan.

Similar trends were observed for the wetting envelopes of the different samples (as shown in Fig. 7). The wetting envelope, which can be used for predicting the wettability of the materials surface, was calculated through the surface energy of the solid material using the Fowkes equation. The method employed is reported in detail elsewhere

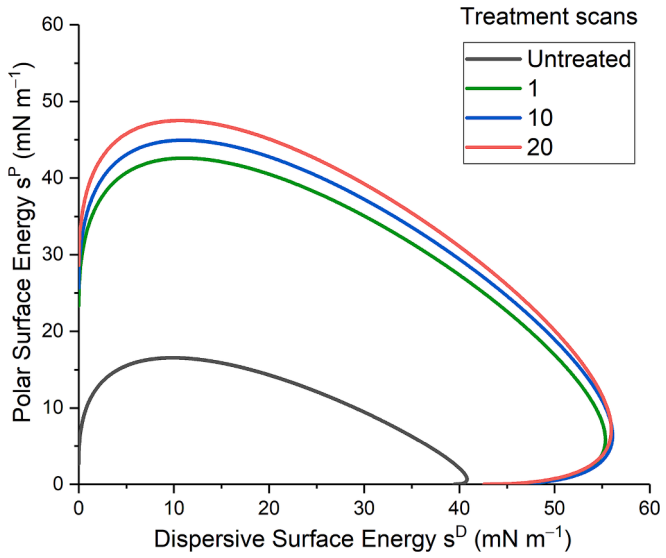

Fig. 7. Wetting envelope of untreated and µPlasma treated GFPA6 surface with different treatment scans.

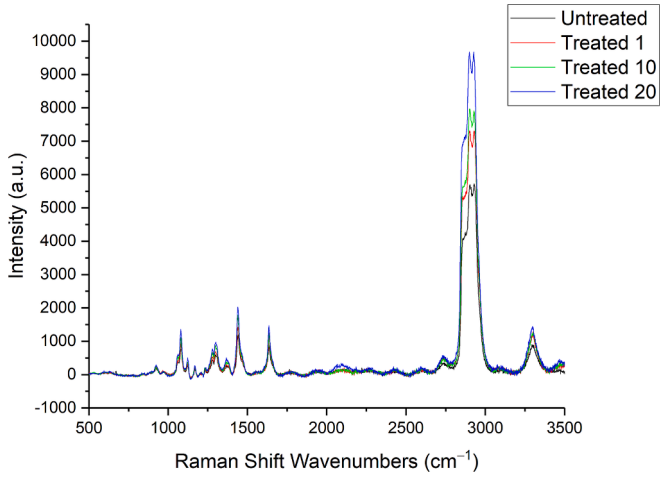

Fig. 8. Raman spectra of untreated GFPA6 and µPlasma treated GFPA6 with different (1, 10, 20) treatment scans.

[20]. When the liquid with surface dispersive σ^D and polar σ^s components are within the values enclosed by the wetting envelope, the liquid is hypothesised to be able to completely wet the surface (i.e., contact angle of 0°). Therefore, larger wetting envelopes indicate better wettability of a sample surface. Fig. 7 revealed that the enclosed area of the wetting envelope increased substantially following a single µPlasma treatment scan. However, only limited increases were found with further increases of the number of µPlasma treatment scans. So clearly, the surface wettability was significantly improved following one µPlasma treatment scan (as demonstrated by the contact angle, surface free energy and wetting envelope data); however, although not detrimental, the influence of further (10 or 20) treatment repetitions did not significantly improve the surface wettability of the GFPA6.

3.3. *Raman spectroscopy*

Analysis of the chemical composition of untreated and µPlasma treated GFPA6 was conducted using Raman spectroscopy, as illustrated in Fig. 8. Three intense peaks were observed in the untreated material between the Raman shifts of 2800 to 3000 cm^{-1}, which were assigned to symmetric and asymmetric vibrations of CH_2 moieties of the polymer.

Table 1
The observed assignments of major Raman peaks of GFPA6 in different wavenumbers [22,23].

Wavenumber (cm^{-1})	Assignments
1060–1129	C–C stretching
1450	CH_2 bending
1646	C = O stretching
2865	Symmetric CH_2
2912	Symmetric CH_2
2936	Asymmetric CH_2
3307	N–H stretching

The band centred at 1093 cm^{-1} was attributed to C–C stretching, while the bands at 1450 cm^{-1} and 1646 cm^{-1} were attributed to CH_2 bending and C = O stretching in amide groups, respectively. N–H stretching of the amides was also observed at a Raman shift of 3307 cm^{-1}. A list of the Raman shifts of the major peaks and their assigned chemical vibrations are reported in Table 1.

Profound increases of the major bands were observed after μPlasma treatment, which indicated that the chemical composition on the surface of the GFPA6 was altered by the μPlasma treatment. A significant increase of the intensity of the symmetric and asymmetric CH_2 peaks were observed with increasing numbers of μPlasma treatment scans. The effect of the treatment on the polar amide groups is shown in Fig. 9, where again, a pronounced increase with treatment number was apparent.

The average intensity of the amide bands increases with the number of the μPlasma treatment scans. The most significant intensity increase is found following the first μPlasma treatment scan, with more subtle increases for 10 and 20 treatment scans.

Raman mapping was used to reveal the distribution of the amide bands across a 2550 × 2550 μm^2 area of the surface of each sample group. Colour heat maps in Fig. 10, average intensity and standard deviation of the amide bands in Fig. 11, and quantitative data (of the averaged intensities and ranges of each map) in Table 2 are used to

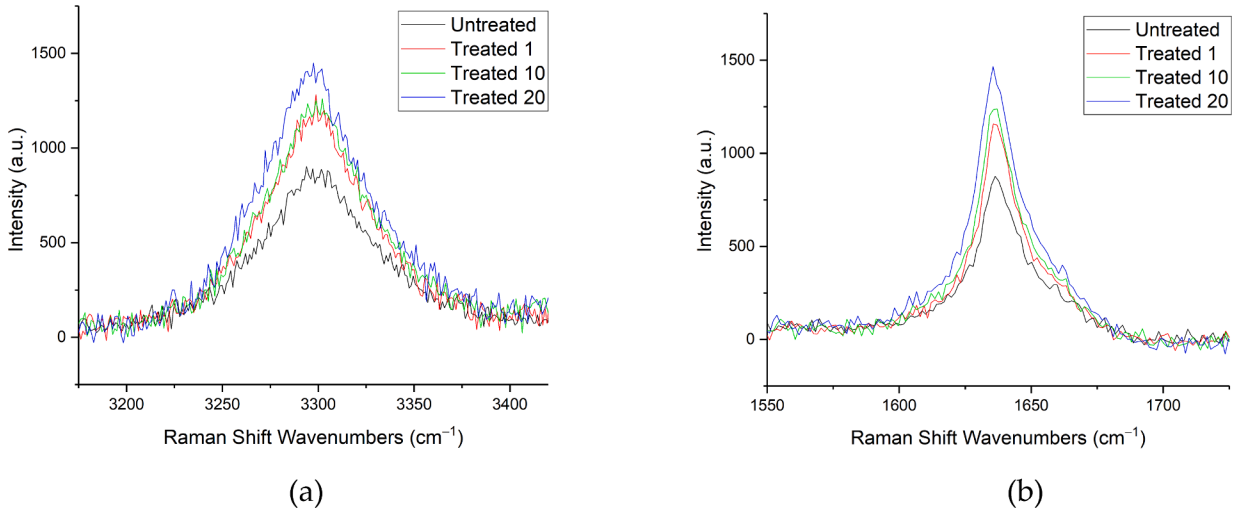

Fig. 9. Raman spectra of GFPA6 in (a) wavenumber 3307 cm^{-1} (N–H stretching), and wavenumber 1646 cm^{-1} (C = O stretching) untreated and μPlasma treated GFPA6 with different (1, 10, 20) treatment scans.

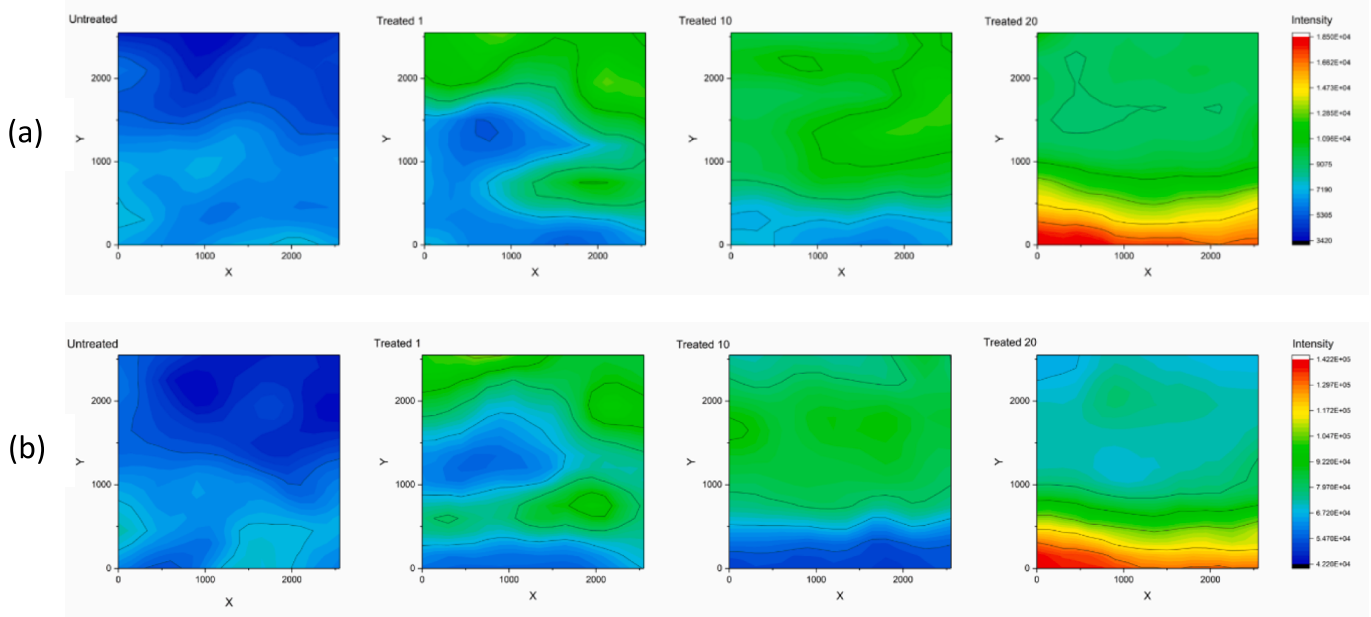

Fig. 10. Distribution of the (a) C = O stretching in the wavenumber of 1646 cm^{-1}, and (b) N–H stretching in wavenumber of 3307 cm^{-1} on the untreated and μPlasma treated sample surfaces (with 1, 10 and 20 treatment scans) with size of 2550 × 2550 μm represented by heat colour mapping.

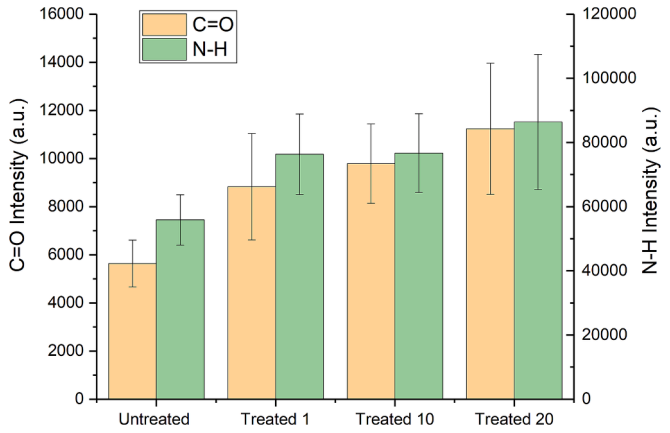

Fig. 11. Average intensity and standard deviation of the amide bands on the untreated and μPlasma treated (with 1,10 20 treatment scans) on the sample surface.

convey and analyse the mapping data. Despite the low average intensity under Raman mapping, homogenous coverage of the polar amide groups was revealed on the surface of the untreated GFPA6 (shown in Fig. 10). As shown in Fig. 11 and Table 2, the average intensity increased by 56.6 % for C = O stretching and 35.6 % for N–H stretching following one μPlasma treatment scan. Considering the magnitude of the increase in the number of scans, the change in average intensity produced after 10 scans was less pronounced compared to one, especially for the N–H stretching (which only increased from 35.6 % to 37.1 %). The peak intensity range was observed to widen following one μPlasma treatment scan (Fig. 10), going from 4201.6 to 7607.6 for C = O stretching and from 30746.4 to 51509.6 for N–H stretching, which indicates heterogeneous distribution bands across the surface. However, when the number of scans was increased to 10, the amide bands appeared to become more homogeneous across the majority of the surface, as the range of intensity decreased to 6342.4 for C = O stretching and 43809.2 for N–H stretching. Significant segregation of the two bands was then found after 20 μPlasma treatment scans, as evidenced by the significant increased intensity range to 9552.6 for C = O stretching and 76493.4 for N–H stretching.

3.4. Adhesive bonding of GFPA6

Fig. 12 shows a comparison of the tensile shear strength of untreated and μPlasma treated GFPA6. Following a single μPlasma treatment scan, a substantial increase in tensile shear strength from 1003.2 N to 1788.1 N was observed. The tensile shear strength was found to further increase to 2268.1 following 10 μPlasma scans (almost double the tensile shear strength of the untreated GFPA6). However, further increases of the number of μPlasma scans did not result in further improvement of the tensile shear strength, with the strength increasing by only 25.4 N (as compared with 10 scans), which is in contrast to the effect of μPlasma treatments on the surface roughness, where the roughness is found to increase substantially with 20 μPlasma treatment scans.

Illustrative fracture surfaces are shown in Fig. 13. In the untreated samples, due to the weak bonding of the adhesive to the polymer surface, the coverage of the adhesive residue on the polymer surface was very limited, but with increased treatment scans, more adhesive was retained on the polymer surface. Analysis of the surfaces revealed that

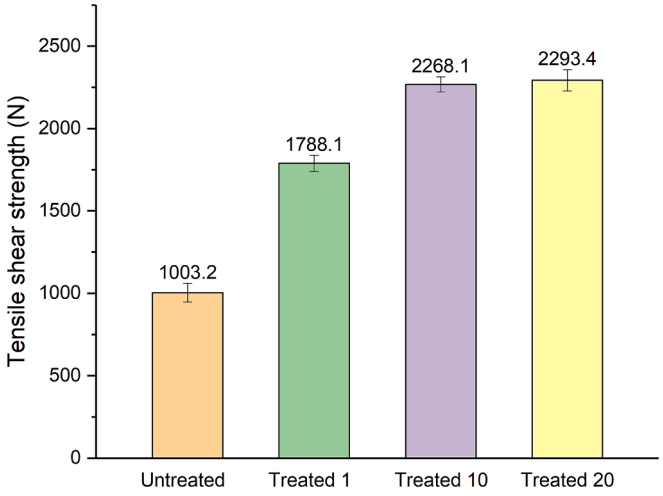

Fig. 12. The tensile shear strength of the bond between GFPA6 and aluminium in different conditions (untreated and μPlasma treated with 1, 10 and 20 treatment scans) and AA-6082 using epoxy adhesive.

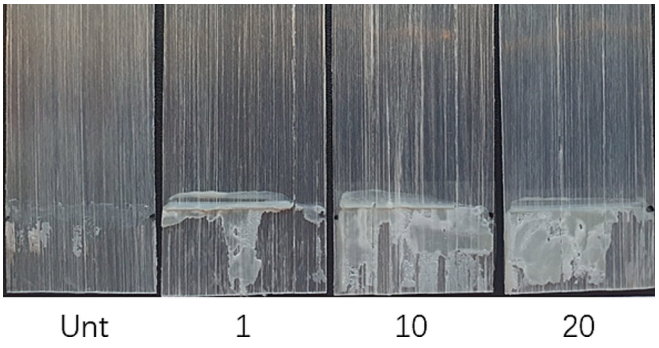

Fig. 13. Image of distribution of adhesive residue on the Untreated GFPA6 and μPlasma treated 1, 10 and 20 scans after tensile lap-shear test failure.

Table 3
Area covered by the residual adhesive on the sample surface.

Treatment	Area%
Untreated	12.2
Treated 1	29.8
Treated 10	83.9
Treated 20	81.2

Table 2
Average intensity and range of intensity across the area.

Bands	Treatment scans	Change in average intensity (%)	Average intensity (a.u.)	Standard deviation (±)	Range of intensity
C = O stretching	0	0	5639.5	973.2	4201.6
	1	56.6	8829.8	2204.9	7607.6
	10	73.5	9787.3	1645.7	6342.4
	20	99.3	11239.0	2724.2	9552.6
N–H stretching	0	0	55906.0	7839.4	30746.4
	1	35.6	75829.0	12560.8	51509.6
	10	37.1	76636.9	12274.0	43809.2
	20	54.5	86386.1	21030.1	76493.4

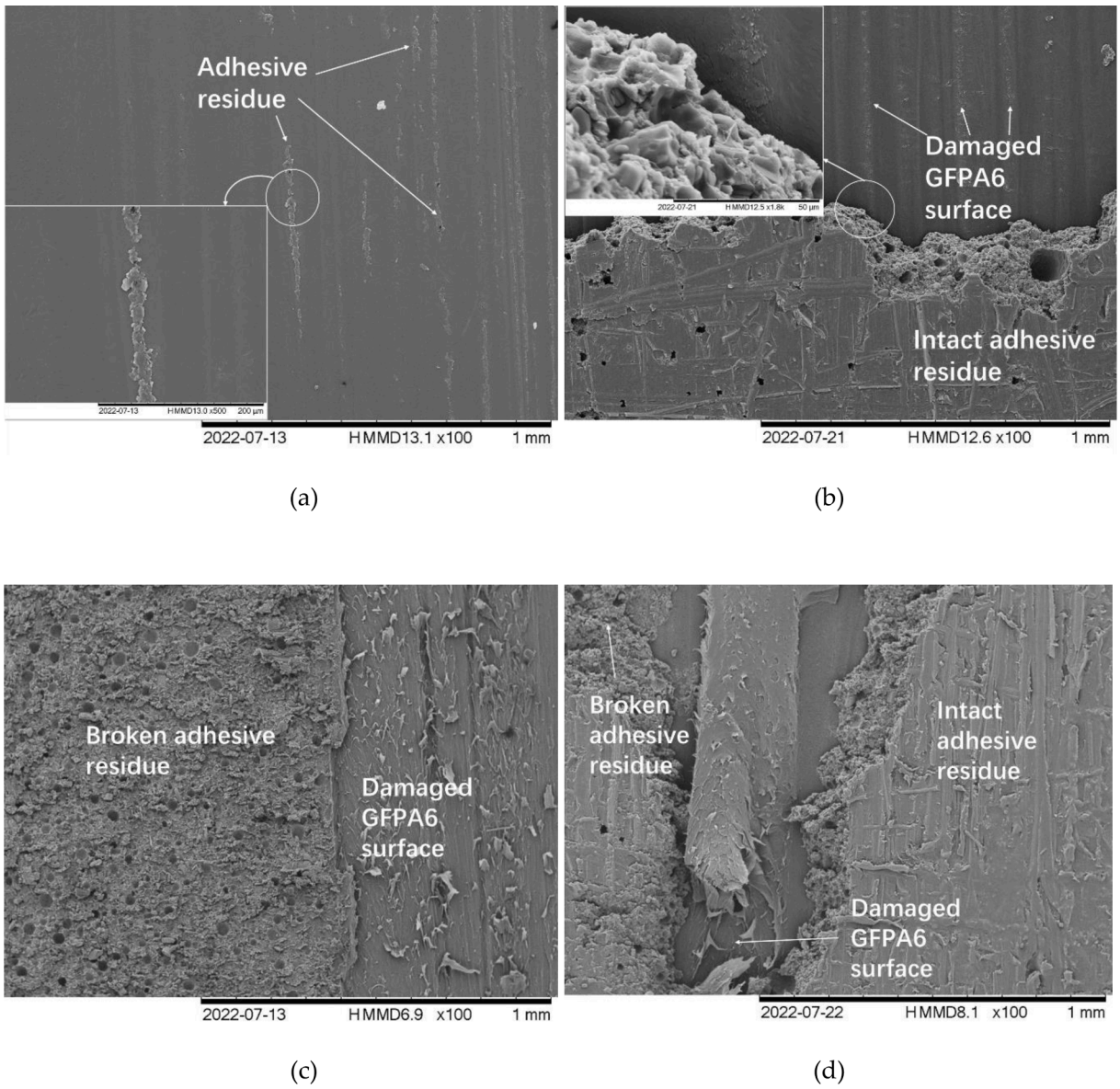

Fig. 14. SEM images of tensile fracture GFPA6 surfaces of (a) untreated, and μPlasma treated different scans: (b) 1 scan, (c) 10 scans and (d) 20 scans.

following a single μPlasma treatment scan, the percentage coverage of the residual adhesive on the polymer surface increased from 12.2 % (untreated) to 29.8 % (shown in Table 3). Intact regions of adhesive were found to peel away from the aluminium sheet (as shown by the smooth adhesive surfaces), therefore indicating that the adhesive bonding between the GFPA6 surface and epoxy adhesives had improved after μPlasma treatment. When 10 μPlasma treatment scans were performed on the sample surface, the amount of adhesive residue increased significantly, covering the majority of the previously joined surface (83.9 %). The amount of the adhesive residue was similar (81.2 %) when 20 μPlasma treatment scans were applied.

Fig. 14 shows the fracture surfaces as recorded by SEM. In the untreated samples (as shown in Fig. 14a with magnified image), there is little evidence of adhesion of the epoxy to the polymer surface (consistent with adhesive failure), however, there is some limited evidence of thin striations of adhesive residue on the fibres (suggesting highly localised thin-layer cohesive failure).

However, following a single μPlasma treatment scan of the GFPA6 surface, damage of the surface became apparent, coupled with some residual adhesive on the surface (Fig. 14 b with magnified image). This surface damage was attributed to the pull force that generated by the improved bonding between the sample surface and the epoxy adhesive during the tensile failure, suggesting a higher bonding strength.

When the number of treatment scans increased to 10 and then 20 (Fig. 14 c and d), more extensive adhesive residue coverage was observed. Damaged adhesive layers were observed on both 10 and 20 μPlasma scanned surface. These layers presented with coarse structures and round pits, likely developed from air bubbles formed when the resin and hardener were mixed. In addition, damage and deformation were revealed of the GFPA6 material surface as a result of strong tensile forces, which indicate that this part of bonding failure was due to substrate failure.

As noted above, the effects of μPlasma surface treatment have been found to be non-permanent and post-treatment ageing occurs. Therefore, in this study, adhesive bonding was expedited to ensure that little or no ageing had occurred prior to joining of the surfaces. The GFPA6 samples were μPlasma treated and joined to AA6082 according to the protocol described in §2.5. To determine whether the ageing process could still impact the adhesion, the joined GFPA6-epoxy-AA6082 samples were then stored under ambient conditions for 24 days prior to

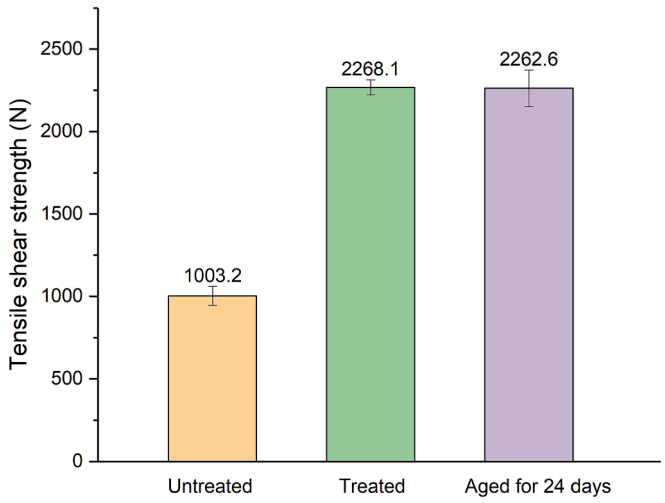

Fig. 15. Comparison of untreated GFPA6-epoxy-AA6082, 10 scans of μPlasma treated GFPA6-epoxy-AA6082, and 10 scans of μPlasma treated GFPA6-epoxy-AA6082 aged in the air for 24 days.

mechanical testing. Compared to the unaged GFPA6-epoxy-AA6082 (whereby the tensile lap-shear test was carried out immediately after joining and curing), the tensile shear strength was found to decrease by only 6.6 N out of 2268.1 N (shown in Fig. 15). This presents a smaller decrease in tensile shear strength than the deviation of the strength data (45.3 N and 110.4 N for the unaged and aged samples respectively). This demonstrates that the 24-day ageing behaviour had negligible effect on the performance of the joined GFPA6-epoxy-AA6082 and that from mechanical test perspective, the ageing process in joined materials is effectively eliminated.

4. Discussion

The μPlasma treatment has been demonstrated to be able to both physically and chemically modify the polymer surface, as indicated by the measurement of roughness and surface wettability. The increase in roughness can be attributed to the process of ablation in which polymeric material is lost from the surface [24]. While increasing the number of treatment scans clearly increased the roughness, the effect was relatively limited for a single treatment scan (a 15.6 % increase in RMS roughness). Studies have shown that a change in roughness on a sample surface plays an important role in determining its wettability [25,26]. However, in this study, it was found the change in wettability of the GFPA6 surface (using contact angle, surface free energy and wetting envelope measurements) did not increase in proportion to the change in surface roughness (as shown in Fig. 16). Although the contact angles were found to substantially reduce (61.5 %) following one μPlasma treatment scan, further decreases in the measured contact angle were limited for 10 and 20 μPlasma treatment scans despite their significantly greater surface roughnesses. Similar trends were also observed in surface free energy and wetting envelope.

The addition of functional groups on solid substrate surfaces has been shown to be able to enhance the adhesion properties of surfaces [27,28]. A study by Ahmed et al. [29] demonstrated enhanced adhesive bonding between polyether ether ketone (PEEK) and aluminium alloy surfaces following the plasma introduction of polar functional groups on the PEEK. This confirmed the positive impact that polar functional groups can play on the chemical interactions of the surface with adhesives. In this present study, μPlasma treatments have been measured to result in increased peak intensities corresponding to the numerous polar groups, including C = O and N–H bonds. As shown in Fig. 16, the largest increase of intensity of the C = O group developed following a single μPlasma treatment (with increases to 10 and 20 scans showing more subdued increases), which also corresponds with the wettability findings. Therefore, given the above observations it is apparent that in this instance, wettability appears to be primarily controlled by the presence of polar functional groups on the surface and not by the surface roughness.

The results from the tensile lap-shear tests indicated that the bonding strength of GFPA6-epoxy-AA6082 increased significantly following μPlasma treatment of the GFPA6 surface. The measured tensile shear strength was found to progressively increase up to 10 treatment scans, with no discernible improvement in bonding strength when the number of scans were increased to 20. Given the significant increases of both surface energy and surface functional groups (as indicated by the intensity of the C = O in Fig. 16) up to 10 scans, it can be implied that

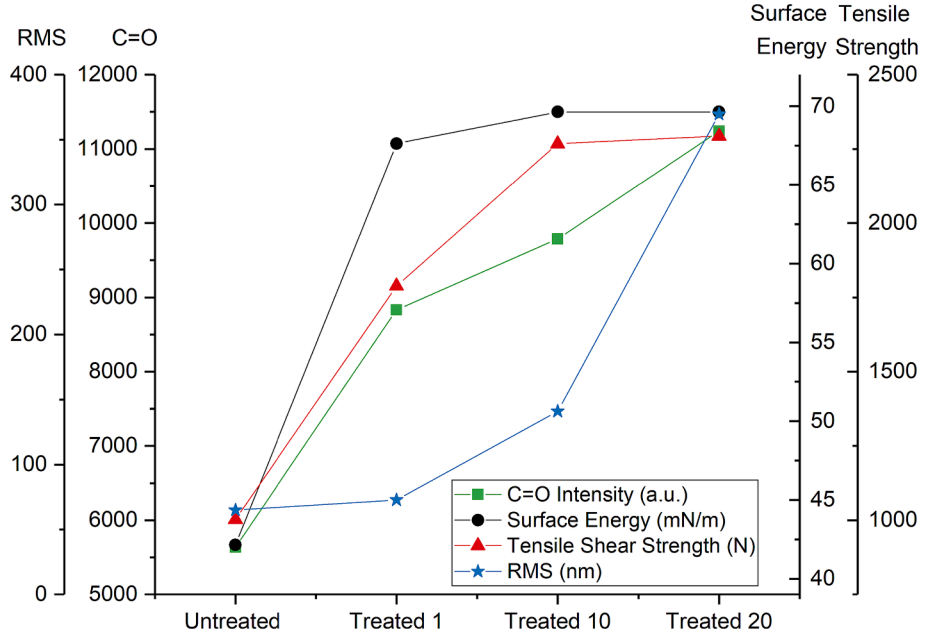

Fig. 16. Comparison of the change in C = O intensity, surface energy, tensile shear strength and RMS of untreated and μPlasma treated (with 1, 10 and 20 scans) GFPA6.

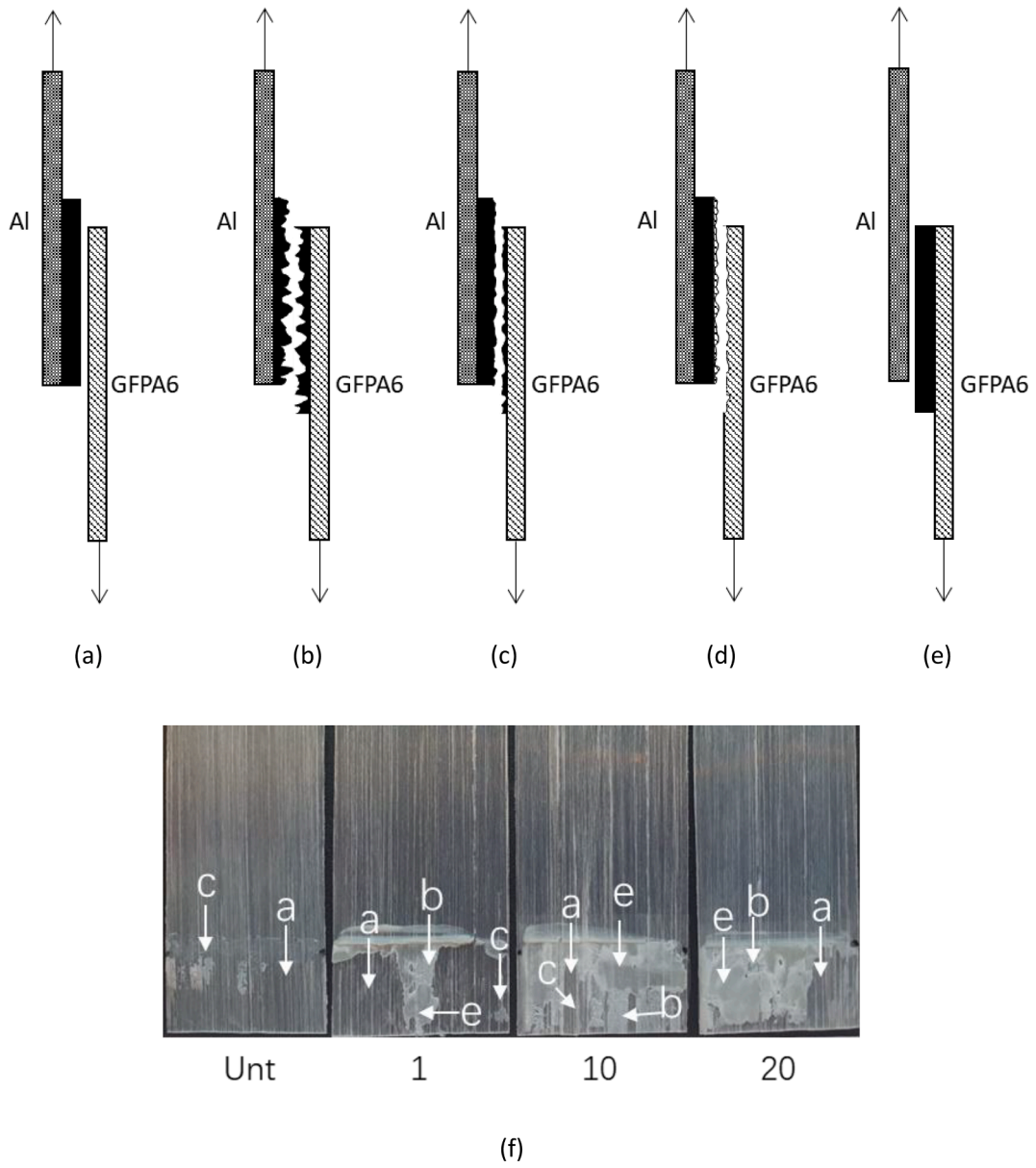

Fig. 17. Illustration of failure mode that happened when broken: (a) adhesive failure of GFPA6, (b) cohesive failure, (c) thin-layer cohesive failure, (d) light-tear failure, (e) adhesive failure of Al and (f) different failure modes distributed on GFPA6 surface after fracture.

surface wettability and the presence of functional groups correlate with the final bonding strength. Therefore, as the maximum intensity of the surface functional groups was found with 20 treatment scans, the expectation was that the strongest and most intimate bonding would develop for these surfaces. However, both 10 and 20 μPlasma treated surfaces were measured to have similar tensile shear strengths, which suggests that other parameters also influence the final bonding strength.

Under small (or negligible) roughness changes (i.e., going from untreated to 1 μPlasma treatment scan), it appears that it is possible to significantly enhance the bonding strength predominantly from the formation of surface functional groups and the enhanced wettability. Similarly, under large roughness changes (i.e., going from 10 to 20 μPlasma treatment scans), it appears that surface roughness either does not positively influence the bonding strength or appears to have a negatively impact. Given the strong etching of the GFPA6 surface with 20 treatment scans, as evidenced by the exposure of the fibres on the surface and the formation of distinct grooves between them (as shown in Fig. 3 d), it is possible that this radical change in surface morphology may have negative influence on the bonding strength with the epoxy adhesive (potentially by forming crevices that have tendencies to trap air). However, further investigations are necessary to explore the influence of surface conditions on the intimacy and strength of bonding with the epoxy adhesive to determine the cause.

The analysis of the surface morphology of GFPA6 after fracture confirms that μPlasma treatments can enhance the surface bonding of GFPA6-epoxy-AA6082, as can be seen the failure modes illustrated in Fig. 17 and the surface morphology observed in Fig. 14. It was shown on the untreated GFPA6 surface that the majority of the adhesive had been completely removed following the tensile lap-shear test, which is consistent with adhesive failure and some (limited) cohesive failure mode and suggests poor bonding. The degree of adhesive remaining on the material surface increased substantially with increasing numbers of μPlasma scans. A mix of light-tear adhesion and thin-layer cohesion failure modes were observed after single μPlasma treatments of the GFPA6 surface, which suggested stronger bonding with the epoxy resin. Moreover, the portions of the surface which were composed of intact adhesive with a smooth surface indicated the initiation of adhesive failure between the epoxy surface and the aluminium surface. After 10

and 20 μPlasma treatment scans, broken adhesives and stretching of the GFPA6 substrate was observed, accompanied by more complex mixtures of failure modes, including adhesive, cohesive, thin-layer cohesive, light-tear and fibre-tear failure modes, which also imply substantial enhancement of the bonding strength. Additionally, significantly greater coverage of smooth intact epoxy resin could be observed on the 10 and 20 scanned surfaces, which also indicate that the load at failure of the tensile lap-shear test was more strongly related to the strength and quality of adhesion between the aluminium surface and the epoxy-resin. This shift in failure mode supports the measured enhancement of surface functionality and wettability.

Interestingly, as the number of μPlasma treatment scans increased from 10 to 20, no significant change in the tensile shear strength could be measured and the fracture surface morphology was not significantly altered, which are both consistent with the observed changes in wettability. The 10 μPlasma treated surface reveals largely homogeneous coverage of the epoxy resin on the GFPA6 surface, which implies that the bonding between the GFPA6 and the epoxy resin did not contribute to the dominating failure modes of the GFPA6-epoxy-AA6082 joint. Instead, the most prominent failure modes appear to be adhesive failure with the aluminium surface (smooth intact epoxy resin) and cohesive failure within the resin (fractured and rough epoxy surface). Interestingly, the 20 μPlasma treated surface does not present with significant increase in the adhesive failure from the aluminium surface, but instead presents with the return of adhesive failure on the GFPA6 surface. As shown in Fig. 3 d (exposure of the glass fibres under AFM imaging) and Fig. 16, the significant change in surface morphology of the 20 treatment scanned surfaces appear to negatively impact the bonding state with the epoxy adhesive. This is further supported by the Raman mapping of the C = O and N–H bonds of the surfaces (Fig. 10), which reveal the formation of regions with significantly greater presence of functional groups. It is possible that these regions correspond to the exposure of the fibres (following the repeated plasma etching of the surfaces following 20 scans) and therefore changing of the bonding environment. In addition to changing the surface morphology, there is potential for the exposed glass fibres to disproportionately load the interface and negatively impact the bonding strength. Overall, the indicates that the homogeneity of the polar groups on the surface is more essential than higher intensity of the peaks for enhancing the bonding strength of GFPA6-epoxy-AA6082, which supports that the bonding strength correlates closely with the water wettability (that relates to polar functional groups). This can explain why the increase in the homogeneity of polar groups plays an important role in enhancing the tensile strength when the μPlasma treatment increased from 1 to 10 scans.

Once adhered, a storage period of 24 days did not appear to significantly influence the bonding strength of the of GFPA6-epoxy-AA6082 sample. This suggests that the epoxy adhesive can form permanent bonds with the functional groups introduced on the surface after μPlasma treatment, thereby preventing the reorientation or diffusion of polar moieties back to into the bulk of the GFRPA6 sample (hydrophobic recovery [30,31]).

5. Conclusion

This study has shown that μPlasma surface treatment of glass fibre reinforced polyamide 6 is highly beneficial in terms of the effectiveness of the adhesive bond with aluminium. Bond strength was found to increase with the number of treatment scans, but no more than ten scans was found to be the optimum. The increase in bond strength was attributed to increases in the following material characteristics; surface energy, polarity and roughness, but the dominant factor that affected the bond strength was deemed to be the increased polarity of the polymer surface. Of key importance in this study was the immediate fabrication of the test sample post-treatment. This approach ensured the effects of post-treatment ageing were minimised and that the maximum benefit available from the surface treatment was realised. From a commercial perspective, the study has shown that μPlasma surface treatment is sufficiently effective when a relatively low number of treatment scans are employed. This, coupled with the atmospheric nature of the technique, points to great potential as a low-cost, on-line, polymer surface treatment technique.

CRediT authorship contribution statement

Chang Che: Writing – review & editing, Writing – original draft, Visualization, Validation, Software, Methodology, Investigation, Formal analysis, Data curation. **Xueqi Zhu:** Data curation. **Behnam Dashtbozorg:** Writing – review & editing, Validation, Software, Methodology. **Xiaoying Li:** Writing – review & editing, Supervision, Resources, Funding acquisition. **Hanshan Dong:** Writing – review & editing, Supervision, Resources, Project administration, Funding acquisition, Conceptualization. **Mike J. Jenkins:** Writing – review & editing, Supervision, Resources, Conceptualization, Project administration.

Declaration of competing interest

The authors declare that they have no known competing financial interests or personal relationships that could have appeared to influence the work reported in this paper.

Data availability

Data will be made available on request.

Acknowledgements

This work was financially supported from the Centre for Doctoral Training in Innovative Metal Processing (IMPaCT) funded by the UK Engineering and Physical Sciences Research Council (EPSRC), grant reference EP/F006926/1, and European Commission (EC ERDF_Smart Factory Hub SmartFub).

References

[1] D. Haber. Lightweight materials for automotive applications: a review. (2015).
[2] W. Zhang, J. Xu, Advanced lightweight materials for Automobiles: A review, Mater. Des. (2022) 110994.
[3] P. Mallick, Thermoplastics and thermoplastic–matrix composites for lightweight automotive structures. Materials, design and manufacturing for lightweight vehicles, Elsevier (2021) 187–228.
[4] R. Bernatas, S. Dagréou, A. Despax-Ferreres, A. Barasinski, Recycling of fiber reinforced composites with a focus on thermoplastic composites, Clean. Eng. Technol. 5 (2021) 100272.
[5] M. Biron, Thermoplastics and thermoplastic composites, William Andrew, 2018.
[6] D. Vlasveld, P. Parlevliet, H. Bersee, S. Picken, Fibre–matrix adhesion in glass-fibre reinforced polyamide-6 silicate nanocomposites, Compos. A Appl. Sci. Manuf. 36 (1) (2005) 1–11.
[7] X.-F. Wei, K.J. Kallio, S. Bruder, M. Bellander, R.T. Olsson, M.S. Hedenqvist, High-performance glass-fibre reinforced biobased aromatic polyamide in automotive biofuel supply systems, J. Clean. Prod. 263 (2020) 121453.
[8] R. Naik, S. Panda, V. Racherla, A new method for joining metal and polymer sheets in sandwich panels for highly improved interface strength, Compos. Struct. 251 (2020) 112661.
[9] A. Pramanik, A. Basak, Y. Dong, P. Sarker, M. Uddin, G. Littlefair, et al., Joining of carbon fibre reinforced polymer (CFRP) composites and aluminium alloys–A review, Compos. A Appl. Sci. Manuf. 101 (2017) 1–29.
[10] A. Galińska, C. Galiński, Mechanical joining of fibre reinforced polymer composites to metals—a review. Part II: riveting, clinching, non-adhesive form-locked joints, pin and loop joining, Polymers 12 (8) (2020) 1681.
[11] R.W. Messler, Joining of materials and structures: from pragmatic process to enabling technology, Butterworth-Heinemann, 2004.
[12] C. Fuentes, L.Q.N. Tran, M. Van Hellemont, V. Janssens, C. Dupont-Gillain, A. W. Van Vuure, et al., Effect of physical adhesion on mechanical behaviour of bamboo fibre reinforced thermoplastic composites, Colloids Surf. A Physicochem. Eng. Asp. 418 (2013) 7–15.
[13] G. Wade, W. Cantwell, Adhesive bonding and wettability of plasma treated, glass fiber-reinforced nylon-6, 6 composites, J. Mater. Sci. Lett. 19 (20) (2000) 1829–1832.

[14] K.S. Kim, C.M. Ryu, C.S. Park, G.S. Sur, C.E. Park, Investigation of crystallinity effects on the surface of oxygen plasma treated low density polyethylene using X-ray photoelectron spectroscopy, Polymer 44 (20) (2003) 6287–6295.
[15] T. Desmet, R. Morent, N. De Geyter, C. Leys, E. Schacht, P. Dubruel, Nonthermal plasma technology as a versatile strategy for polymeric biomaterials surface modification: a review, Biomacromolecules 10 (9) (2009) 2351–2378.
[16] Z. Gao, J. Sun, S. Peng, L. Yao, Y. Qiu, Surface modification of a polyamide 6 film by He/CF4 plasma using atmospheric pressure plasma jet, Appl. Surf. Sci. 256 (5) (2009) 1496–1501.
[17] J. Ku, I. Jung, K. Rhee, S. Park, Atmospheric pressure plasma treatment of polypropylene to improve the bonding strength of polypropylene/aluminum composites, Compos. B Eng. 45 (1) (2013) 1282–1287.
[18] A. Carradò, O. Sokolova, B. Donnio, H. Palkowski, Influence of corona treatment on adhesion and mechanical properties in metal/polymer/metal systems, J. Appl. Polym. Sci. 120 (6) (2011) 3709–3715.
[19] A. Mameli, Y. Kuang, M. Aghaee, C.K. Ande, B. Karasulu, M. Creatore, et al., Area-selective atomic layer deposition of In2O3: H using a μ-plasma printer for local area activation, Chem. Mater. 29 (3) (2017) 921–925.
[20] C. Che, B. Dashtbozorg, X. Li, H. Dong, M. Jenkins, Effect of μPlasma Modification on the Wettability and the Ageing Behaviour of Glass Fibre Reinforced Polyamide 6 (GFPA6), Materials 14 (24) (2021) 7721.
[21] B. Standard, Paints and varnishes — Wettability. Part 2: Determination of the surface free energy of solid surfaces by measuring the contact angle, BSI Standards Publication, 2020.
[22] H. Uematsu, T. Kawasaki, K. Koizumi, A. Yamaguchi, S. Sugihara, M. Yamane, et al., Relationship between crystalline structure of polyamide 6 within carbon fibers and their mechanical properties studied using micro-raman spectroscopy, Polymer 223 (2021) 123711.
[23] W. Maddams, I. Royaud, The application of Fourier transform Raman spectroscopy to the identification and characterisation of polyamides—II. Double-number nylons, Spectrochim. Acta A: Mol. Spectrosc. 47 (9–10) (1991) 1327–1333.
[24] E. Baburaj, D. Starikov, J. Evans, G. Shafeev, A. Bensaoula, Enhancement of adhesive joint strength by laser surface modification, Int. J. Adhes. Adhes. 27 (4) (2007) 268–276.
[25] H.B. Baniya, R.P. Guragain, B. Baniya, D.P. Subedi, Cold atmospheric pressure plasma jet for the improvement of wettability of polypropylene, Int. J. Polym. Sci. 2020 (2020).
[26] F. Rupp, L. Scheideler, D. Rehbein, D. Axmann, J. Geis-Gerstorfer, Roughness induced dynamic changes of wettability of acid etched titanium implant modifications, Biomaterials 25 (7–8) (2004) 1429–1438.
[27] A. Carré, V. Lacarrière, How substrate properties control cell adhesion. A physical–chemical approach, J. Adhes. Sci. Technol. 24 (5) (2010) 815–830.
[28] F. Awaja, M. Gilbert, G. Kelly, B. Fox, P.J. Pigram, Adhesion of polymers, Prog. Polym. Sci. 34 (9) (2009) 948–968.
[29] A. Khan, F. Liu, P. Dong, Joining of metal and non-polar polypropylene composite through a simple functional group seeding layer, J. Manuf. Process. 85 (2023) 90–100.
[30] V. Jokinen, P. Suvanto, S. Franssila, Oxygen and nitrogen plasma hydrophilization and hydrophobic recovery of polymers, Biomicrofluidics 6 (1) (2012) 016501.
[31] E. Bormashenko, G. Chaniel, R. Grynyov, Towards understanding hydrophobic recovery of plasma treated polymers: storing in high polarity liquids suppresses hydrophobic recovery, Appl. Surf. Sci. 273 (2013) 549–553.